Available online at www.sciencedirect.com
SCIENCE DIRECT®
Journal of Nuclear Materials 325 (2004) 148–158
journal of nuclear materials
www.elsevier.com/locate/jnucmat

Helium thermal diffusion in a uranium dioxide matrix

Danièle Roudil [a,*], Xavier Deschanels [a,1], Patrick Trocellier [b,2], Christophe Jégou [a,3], Sylvain Peuget [a,4], Jean-Michel Bart [a,5]

[a] CEA VALRHO Marcoule, DEN/DIEC/SESC/LMPA, B.P. 17171, 30207 Bagnols-sur-Cèze cedex, France
[b] CEA SACLAY, DEN/DMN/SRMP, 91191 Gif-sur-Yvette cedex, France

Received 11 July 2003; accepted 27 November 2003

Abstract

The behavior of helium and its diffusion mechanisms in uranium dioxide significantly impact the possible evolution of the spent fuel matrix in interim storage or in a disposal repository, and are therefore an essential aspect of the R&D, regarding fuel matrix behavior in a closed system. A specific experimental study has been conducted, the first part being devoted to thermal diffusion and applied on implanted samples. The analysis procedure used is based on the spreading (under thermal annealing conditions) of a helium-3 profile initially created in the material. The profile is investigated by the resonant nuclear reaction $^3He(d,p)^4He$. The measured helium-3 diffusion coefficients obtained indicate two types of behavior between 1123 and 1273 K, depending on the fluence, with a common activation energy of 2 eV. The values determined experimentally demonstrate that the thermal component of helium diffusion in spent fuel will not be significant over the time/temperature range of interim storage and disposal. Vacancy defects can lead to changes in the behavior and in the diffusion of helium. They will be quantified in the second part of this study.

1. Introduction

The issues of high-level radioactive waste management are extensively investigated throughout the world and notably in France by the *Commissariat à l' Énergie Atomique* (CEA). Long term interim storage and geological disposal of spent nuclear fuel is being investigated within the framework of the December 1991 radioactive waste management act for the management of spent fuel in the back-end of the cycle. One of the major operational R&D questions concerns the monitoring of spent fuel packages in storage and the applicability of potential reconditioning processes. Studying the long-term behavior of UO_2 and $(U, Pu)O_2$ matrices in a closed system should allow us to identify a radionuclide source term whose variations raise a major operational safety problem in dry interim storage.

One of the consequences arising from the presence of actinides in these materials is the formation of a large quantity of helium produced by α disintegration. The solubility of helium is generally limited in many ceramics. Although it exceeds that of the fission gases Xe and Kr in UO_2, it is still below 0.5%. The solubility limit determined under gas pressure has been estimated as less than 6.7×10^{-4} cm^3 (STP) $(gUO_2)^{-1}$ atm^{-1} [1] and only 2.4×10^{-5} cm^3 (STP) $(gUO_2)^{-1}$ atm^{-1} in monocrystals [2].

This phenomenon leads in particular to microscopic and macroscopic swelling that may result in cracking of the material. A review of the damage induced by

* Corresponding author. Tel.: +33-466 796 172; fax: +33-466 797 708.
E-mail addresses: danielle.roudil@cea.fr (D. Roudil), xavier.deschanels@cea.fr (X. Deschanels), patrick.trocellier@cea.fr (P. Trocellier), christophe.jegou@cea.fr (C. Jégou), sylvain.peuget@cea.fr (S. Peuget), jean-michel.bart@cea.fr (J.-M. Bart).
[1] Tel.: +33-466 796 087; fax: +33-466 797 708.
[2] Tel.: +33-169 088 468; fax: +33-169 086 867.
[3] Tel.: +33-466 791 642; fax: +33-466 797 708.
[4] Tel.: +33-466 796 532; fax: +33-466 797 708.
[5] Tel.: +33-466 796 535; fax: +33-466 797 708.

0022-3115/$ - see front matter © 2003 Elsevier B.V. All rights reserved.
doi:10.1016/j.jnucmat.2003.11.012

irradiation in nuclear ceramics [3] showed the extent of the physical modifications in the matrix.

This effect is generally detrimental to the leaching behavior of nuclear waste containment matrices because it increases the surface area in contact with water. In the case of spent fuel, this phenomenon is accompanied by a significant variation in the source term that must be taken into account to evaluate the radionuclide balance liable to be released if the containment is breached. This study is the first step in an experimental program to determine the behavior of helium in the uranium dioxide matrix, based on characterization and analysis of helium-implanted or actinide-doped materials. The helium diffusion coefficients can be used to quantify the helium fraction that would be released according to the duration of the storage period.

Little published data is available concerning helium diffusion in waste containment matrices, but diffusion coefficients have been reported for UO_2 and PuO_2 by Stark and Rufeh [1,4], nuclear glass [6] and britholite [5]. Our study following the same procedure as [5] consisted of three steps:

- implantation of helium-3 in UO_2 samples,
- annealing of samples at various temperatures to induce helium diffusion,
- measurement of the helium profile in the material by the resonant $^3He(d,p)^4He$ nuclear reaction.

Applications of micro-nuclear reaction analysis (NRA) and its potential for analyzing helium-3 profiles in nuclear ceramics were recently described [7,8]. This is a local nondestructive technique recommended by Paszti [9] using one of two nuclear reactions: $^3He(d,p)^4He$ or $^3He(n,p)^3He$; it has been widely used – particularly with the first reaction – in a variety of solids and has a satisfactory detection limit, as shown by the work reported in [10,11]. Depending on the depth and desired resolution, the backscattered high-energy proton or the recoil ^4He nucleus can be detected.

More recently [12], a similar study was undertaken with samples of zirconolite, a ceramic matrix under consideration for specific conditioning of minor actinidesas an alternative to transmutation after enhanced separation.

In the following paragraphs we describe the sample characteristics, the experimental approach, and the results obtained.

2. Experimental

2.1. Sample characteristics

Depleted (0.2% in ^{235}U) polycrystalline UO_2 pellets were fabricated by the CEA at Cadarache as representative samples of the UOX fuel matrix. As in the industrial process, the pellets were sintered for 4 h at 1700 °C in controlled atmosphere: 95% Ar + 5% humidified H_2. The resulting pellets were then cut into thin disks (about 400 μm thick) and polished.

Table 1
Test pellet characteristics

Mean diameter (mm)	8.197
Mean geometric density	10.3
Mean geometric density (% theoretical density)	94%

The disks were heat treated in dry hydrogen for 4 h at 1500 °C followed by 2 h at 1000 °C with the following objectives:

- restore the material stoichiometry (O/M≈2),
- eliminate any impurities due to polishing,
- eliminate surface defects induced by cutting and polishing.

The characteristics of the test pellets are indicated in Table 1. SEM observation of these samples showed a mean grain size about 10 μm (Fig. 1). The disks were

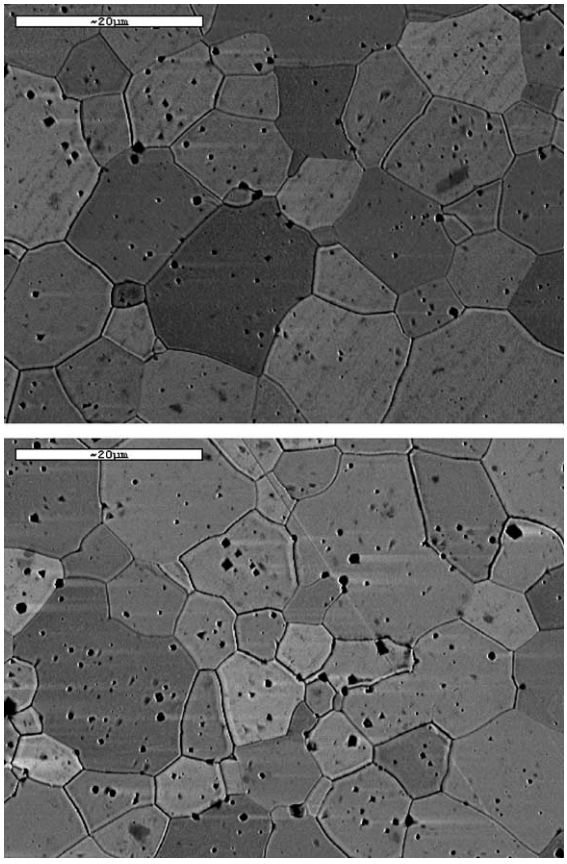

Fig. 1. SEM images of uranium dioxide sample after grain development.

polished on both faces (rugosity lower than 1 μm) and cut into four equal portions.

2.2. Helium-3 implantation and sample annealing

Helium-3 ions were implanted in the materials at room temperature with an energy of 2.9 MeV for the UO_2 samples with fluence values near 3×10^{15} and 3×10^{16} He^+ cm^{-2}. The dose rates were identical for each implantation. Under these conditions, the implantation depth calculated by SRIM2000 was about 6.5 μm; the maximum concentration of the implantation peak was about 0.06 and 0.6 at.%, respectively. Helium concentrations of this magnitude would be obtained after several hundred years of storage in UOX or MOX fuel (Fig. 2).

The implantation was performed using a Van de Graaff accelerator that was unable to cover the full sample surface. Nevertheless, the beam provided a homogeneous flux over a zone 3 mm in diameter at the center of the pellets, and the nuclear microprobe analysis was performed in this zone.

One-fourth of each pellet was reserved as a control specimen to determine the standard deviation of the helium-3 distribution in the untreated sample. The other three fragments were annealed under variable time and temperature conditions to induce helium diffusion (Table 2).

The diffusion coefficients are significantly affected by any deviation from UO_2 matrix stoichiometry; a specific annealing system under neutral atmosphere with an imposed oxygen concentration was therefore used. The annealing furnace scavenged by a gas mixture of $N_2 + 1\%H_2$ included online oxygen partial pressure measurement provisions to monitor any stoichiometric deviation versus the temperature. The deviations were calculated on the basis of published work in this area, notably [13,14]. The oxygen partial pressure was imposed by the water dissociation reaction, according to the principles and model discussed in [15]. The process (Fig. 3) was used to apply the annealing conditions shown in Table 2, clearly indicating the very limited deviation from the stoichiometric ratio.

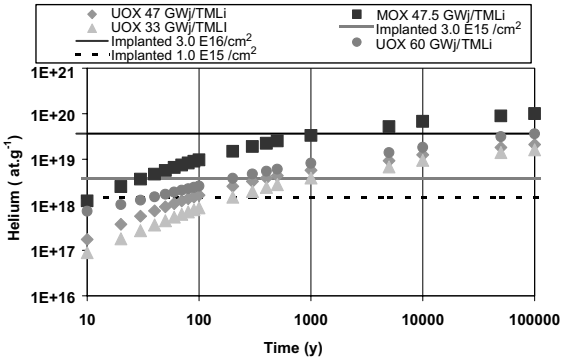

Fig. 2. Comparison between helium generated in spent fuel and the implanted samples studied.

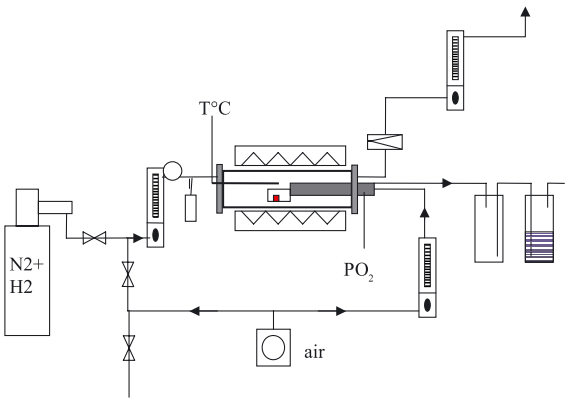

Fig. 3. Schematic view of controlled atmosphere annealing device.

2.3. Determination of the helium 3 profiles

The helium-3 profile was measured by the $^3He(d,p)^4He$ nuclear reaction using the nuclear microprobe in the CEA's Pierre Süe Laboratory at Saclay. This reaction has a maximum cross section for a deuteron energy of 450 keV. During the analysis, the incident deuteron beam energy was progressively reduced from 1500 to 900 keV in variable steps to probe the entire helium-3 profile. The energy step amplitude n, for each acquisition, was adjusted based on the value measured at step $n-1$. The beam intensity was 8 nA and the scanned surface measured 50×50 μm^2; these parameters were optimized to avoid overheating the sample. The protons produced by the $^3He(d,p)^4He$ reaction had an energy of about 13.5 MeV and were collected by a

Table 2
Experimental heat treatment conditions

Temperature (°C)	Duration (H)	$P(O_2)$ (Pa)	Initial mass (g)	Mass after annealing (g)
1000	4	1.1×10^{-14}	0.0554	0.0555
850	48	7.0×10^{-18}	0.0624	0.0623
900	30	7.0×10^{-17}	0.0684	0.0685
950	8	5.5×10^{-16}	0.0621	0.0620

detector comprising three superimposed silicon wafers, each of 500 μm thick, placed on the deuteron beam centerline, and energy resolution of 30 keV. A 25 μm thick mylar energy filter was used to stop the backscattered deuteron and α particles from $^{16}O(d,\alpha)$ reaction.

The total number of protons received by the detector for each deuteron energy level was therefore

$$N_p(E_d) = N_d(E_d)\Omega \int_{x=0}^{\infty} \frac{\sigma_{dH}}{d\Omega}(E_d - g(x))\rho(x)\,dx, \quad (1)$$

where E_d, is the deuteron energy; N_d, number of deuterons of energy E_d reaching the sample; Ω, solid angle of proton detector; $\frac{d\sigma_{dH}}{d\Omega}$, differential cross section of the $^3He(D,p)^4He$ reaction in the test configuration; $E_d - g(x)$, deuteron energy of interaction at depth x; $g(x)$, deuteron deceleration in the material; $\rho(x)$, helium-3 concentration profile (assumed to follow a normal distribution).

Before analysis, all the samples were coated with a 25–30 nm graphite layer.

The analysis method used consists in plotting the curve of the number of protons collected versus the incident deuteron energy for a fixed charge.

2.4. Digital processing of spectral data

Two methods were used to determine the diffusion coefficients and the corresponding activation energy.

A mathematical treatment discussed in [5] for brithholite and based on a least-squares refinement of the curve convoluting the helium-3 implantation profile with the $^3He(d,p)^4He$ reaction cross section was used to obtain the characteristics of the helium-3 profile in uranium dioxide: integrated profile area, depth and width at half maximum.

The incident deuteron stopping power in UO_2 was estimated using SRIM2000 with the data from [16] to establish a polynomial representation used to integrate Eq. (1) numerically as shown in Fig. 4.

The backscattered protons spectra were also analyzed using simulation software (SIMNRA) developed by Matej Mayer and described in [17]. The nuclear reaction cross section was determined by [18] with a deuteron stopping power in UO_2 estimated as above from [16]. After modeling the experimental configurations of the sample and detector, the theoretical overall spectrum was established by superimposing the elementary spectra obtained for each material layer. The contribution of each isotope was calculated in each shell. The calculated values were fit to the experimental spectrum by optimizing the sample representation in terms of the number and thickness of the layers as well as the helium concentration.

Energy calibration, i.e. converting the detection channel number into the deuteron energy, is performed on reference pellets using the $^{16}O(d,p)^{17}O$ and $^{12}C(d,p)^{13}C$ nuclear reactions generating low-energy proton peaks.

The entire profile was thus approximated by a Gaussian curve as is frequently done for implanted profiles ([19,20]):

$$C(x) = \frac{C_0}{\sqrt{2\pi}\sigma} e^{-\frac{(x-x_0)^2}{2\sigma^2}}, \quad (2)$$

where σ is the standard deviation and x_0 the distribution centroid.

The diffusion coefficients were calculated from the spreading of the experimental profiles. The diffusion coefficient is related to the profile width by the following expression:

$$\sigma_T^2 = \sigma_0^2 + 2Dt, \quad (3)$$

where σ_T is the standard deviation of the distribution obtained after annealing for time t at temperature T, σ_0 the standard deviation of the distribution on the unannealed implanted sample, and D the diffusion coefficient.

2.5. Results

The significant drop in the maximum number of protons collected and the overall broadening of the backscattered proton profiles at low fluence (Fig. 5) reveal the diffusion induced by heat treatment at 1000, 900

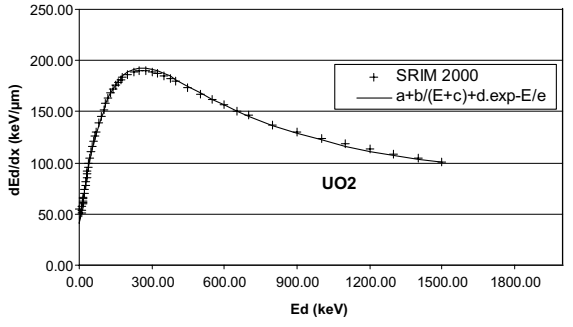

Fig. 4. Modeling of deuteron stopping power in UO_2 by SRIM 2000.

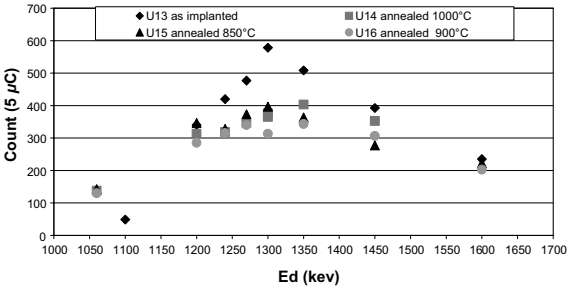

Fig. 5. Number of deuterons collected versus incident deuteron energy for a fluence of 3.0×10^{15} ions cm^{-2}.

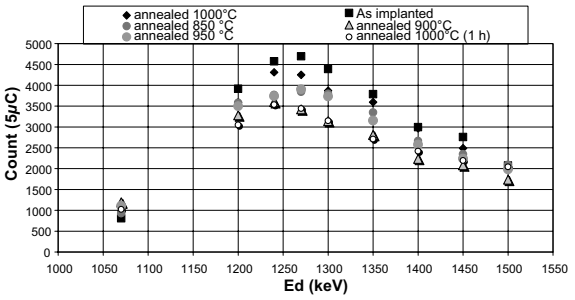

Fig. 6. Number of deuterons collected versus incident deuteron energy for a fluence of 3.0×10^{16} ions cm^{-2}.

and 850 °C. At higher fluence the curves in Fig. 6 also indicate a drop in the maximum number of backscattered protons but much less profile spreading for the same annealing time and temperature.

Furthermore, a shift of the entire profiles towards the surface was always observed on annealed samples. The average value of this shift is about 200 nm.

SIMNRA allows discrete modeling of the sample composition by fitting the number of protons collected per detection channel on the experimental data. These calculations (see examples of results in Fig. 7) are then converted to variations in the helium concentration profiles versus the depth in the material as shown at each fluence in Fig. 8 for all the samples analyzed.. The curves clearly show two different diffusivity behaviors according to the fluence. The effective diffusion constant, deduced from those experiments, according to the relation (3), are presented in Tables 3 and 4.

Thermal diffusion appeared to be significantly affected by the concentration: the diffusion coefficients drop by half an order of magnitude as the concentration increases.

Moreover, after annealing, the remaining ^{3}He content decreased and appeared to be both temperature and time dependant. At low fluence we noted a relative release of about 10% after annealing for 4 h at 1000 °C and a maximum release of 19% after 30 h at 900 °C.

At high fluence, the observed relative release is similar but the fraction values are lower, measured between 5% (1000 °C for 4 h) and 10.3% (850 °C for 48 h). A

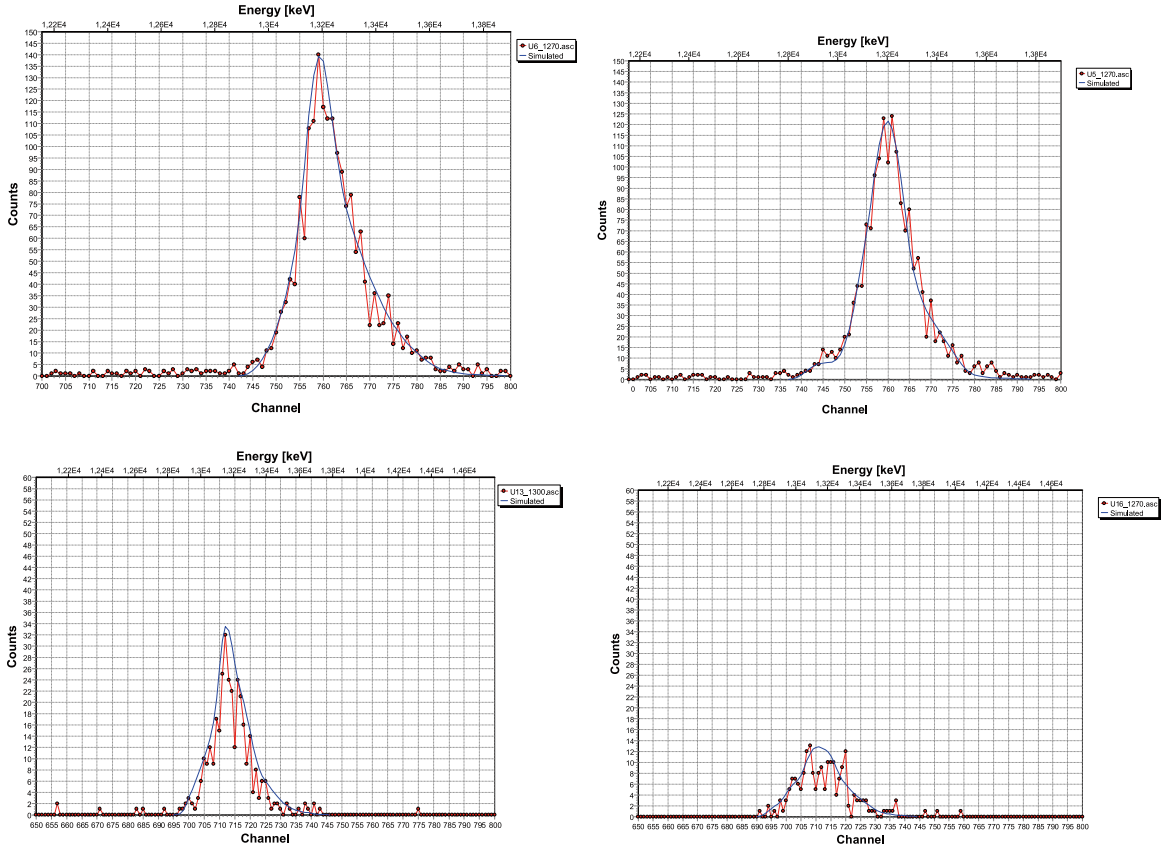

Fig. 7. Helium profiling in samples simulated with SIMNRA and fit to experimental spectra obtained with an incident deuteron energy of 1270 or 1300 keV.

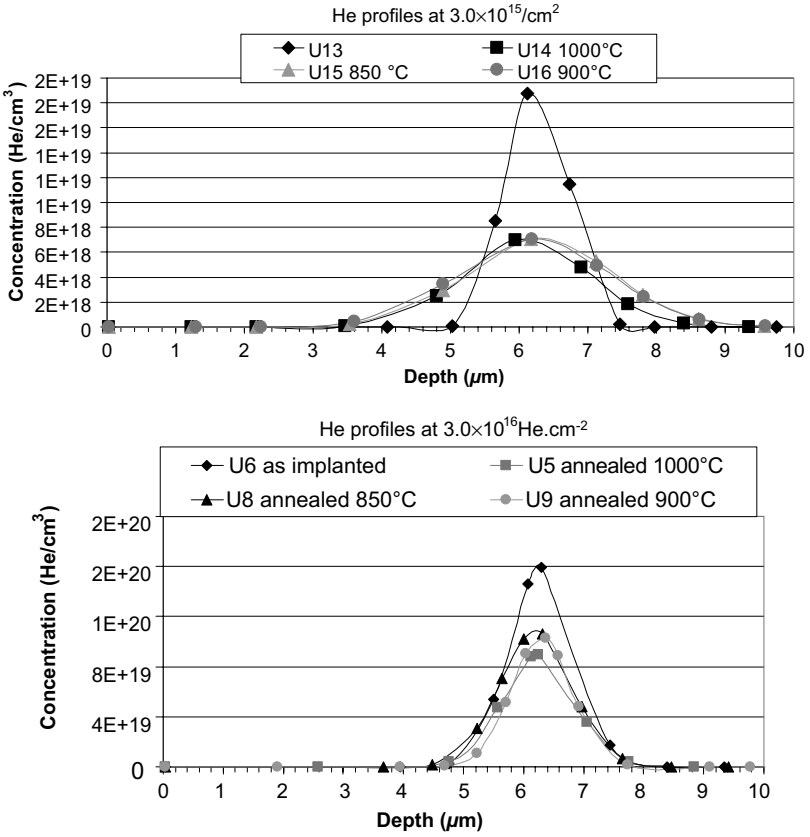

Fig. 8. Implanted helium profile variation after heat treatment versus fluence.

Table 3
Helium diffusion coefficient in UO_2 evaluated by excitation curve method

F (10^{16} He cm^{-2})	T (°C)	Duration (H)	C_0 (10^{16} He cm^{-2})	X_0 (μm)	σ (μm)	D (m^2 s^{-1})
0.3[a]	–	–	0.56	6.5	0.54	–
0.3	1000	4	0.46	6.47	0.93	2.9×10^{-17}
0.3	900	30	0.44	6.29	1.07	3.8×10^{-18}
0.3	850	48	0.48	6.12	1.03	2.2×10^{-18}
3[a]	–	–	4.6	6.06	0.48	–
3	1000	4	4.38	6.01	0.58	3.7×10^{-18}
3	850	48	4.14	6	0.61	4.2×10^{-19}
3[a]	–	–	4.4	6.04	0.46	–
3	950	8	4.06	5.9	0.61	2.8×10^{-18}
3	900	30	4.07	5.9	0.615	7.8×10^{-19}

[a] Indicates reference sample, as implanted and without annealing.

slight difference is nevertheless noticed, depending on the implanted helium quantity.

One experiment was conducted on a sample implanted with a fluence of 3.0×10^{16} He cm^{-2} after annealing for one hour at 1000 °C. The result showed profile broadening, but with an unusual flat shape. The diffusion coefficient values calculated by the two methods were not in agreement depending on the energy of the incident deuteron (between 1270 and 1500 keV). Moreover, the profile shift began but perhaps appeared to be still in progress. Extended tests were not conducted at this temperature.

For NRA, the depth resolution limit is lower than 100 nm. Because the ^{3}He(d,p)^{4}He is a resonant nuclear

Table 4
Helium diffusion coefficient in UO_2 evaluated by the SIMNRA code

F (10^{16} He cm^{-2})	T (°C)	Duration (H)	C_0 (10^{16} He cm^{-2})	X_0 (μm)	σ (μm)	D (m^2 s^{-1})
0.3[a]	–	–	0.37	6.3	0.45	–
0.3	1000	4	0.34	6.1	0.9	2.3×10^{-17}
0.3	900	30	0.33	6.2	1.1	4.8×10^{-18}
0.3	850	48	0.3	5.8	1	2.4×10^{-18}
3[a]	–	–	3.3	6.15	0.5	–
3	1000	4	2.5	5.95	0.56	2.2×10^{-18}
3	850	48	2.56	6.15	0.55	1.6×10^{-19}
3[a]	–	–	2.2	6	0.45	–
3	950	8	1.8	5.9	0.51	1.0×10^{-18}
3	900	30	2.2	5.95	0.52	3.0×10^{-19}

[a] Indicates reference sample, as implanted and without annealing.

reaction, a value of 10 nm is considered. Helium depth profiles were then obtained by numerical simulation in which the integral is discretised with a 20 nm depth step [5]. This resolution limit on σ leads, by differentiating equation (3), to a relative error on D ranging from 3% to 10%, depending respectively on low and high fluence values namely high and small broadening profile.

Similar experiments conducted at a fluence of 1.0×10^{15} He cm^{-2} allow us to examine the detection limit of our measurements. The number of collected protons was very low and cannot lead to accurate diffusivity measurements. At 1000 °C we estimated the value of the diffusion coefficient to be 1.0×10^{-17} m^2 s^{-1}, close to the value obtained before. For the other samples after annealing, the profile broadening and the helium release were too great for the NRA technique.

Nevertheless, these findings indicate that, for an energy of implantation of about 3 MeV, a dose of about 10^{15} He cm^{-2} corresponds to the lower limit for He depth profiling by NRA in UO_2.

3. Discussion

3.1. Thermal diffusion

Considering the grain size (about 10 micrometers) and the relatively narrow distribution of helium ions (about 400 nanometers after implantation) the grain boundaries diffusion phenomenon has a low influence on the global diffusion measured. Nevertheless, peak area measurements compared with the unannealed implantation profile indicate that between 5% and 19% of the total quantity of implanted helium is released; this phenomenon already reaches for the lower temperature and longer treatment duration. It could arise from intergranular diffusion via the grain boundaries, according to processes similar to the release of fission gases [21].

With the release fraction values Re, using the Booth model [22], we can approximate the effective diffusion coefficient D/a^2, where D is the diffusion coefficient and a the radius of the grain (equivalent sphere), during isothermal annealing for a time t, as:

$$3\frac{Dt}{a^2}-\frac{6}{\sqrt{\pi}}\sqrt{\frac{Dt}{a^2}}+Re=0. \tag{4}$$

Results evaluated by this method are presented in Table 5. Despite the limited analysis zone size, two sets of values are again obtained, versus implanted dose.

The decrease of the diffusion coefficients while increasing helium dose was clearly deduced from both numerical data processing methods. This is a significant result considering the measurement sensitivity. The deviation could be related to different mechanisms:

- the precipitation of helium in the material structure, according to helium behavior in UO_2 study at a concentration of 1 at.% presented in [23],

Table 5
Fractional release of helium during isothermal annealing

F (10^{16} He cm^{-2})	T (°C)	Duration (H)	Re (%)	D/a^2 (s^{-1})
0.3	1000	4	10.4	1.1×10^{-7}
0.3	900	30	19	3.4×10^{-8}
0.3	850	48	13	9×10^{-9}
3	1000	4	5	1.6×10^{-8}
3	950	8	7.7	1.9×10^{-8}
3	900	30	8.4	6×10^{-9}
3	850	48	10.3	5.7×10^{-9}

- the effect of defect induced by ions implantation in the material.

Nevertheless, we had never observed increase nor sharpness of the profiles, giving evidence of bubbles. This hypothesis could be validated by TEM observations of this type of sample. Nanometer size bubbles can not be easily detected by the depth profiling method implemented here.

The diffusion coefficient values presented in Tables 3 and 4 concern apparent diffusivity in the matrix, induced by volume diffusion but possibly modified by implantation defects, as discussed later (see Section 3.3).

3.2. Activation energy

The diffusion coefficient is plotted versus the temperature in Fig. 9. The following expression for the helium-3 diffusion coefficients in uranium dioxide was obtained by linear regression:

$$D = D_0 \cdot e^{-\frac{E_a}{KT}} \quad \text{for } 1123 < T < 1273 \text{ K}, \tag{5}$$

where D is the diffusion coefficient ($m^2\,s^{-1}$); D_0, pre-exponential factor ($m^2\,s^{-1}$); E_a, atomic activation energy (eV); K, Boltzmann constant ($eV\,K^{-1}$); T, temperature (K).

This linear regression with a constant slope indicates an activation energy of about 2 eV, depending on the treatment methods (Table 6) and a different Y-intercept depending on the fluence:

$D_0 = 8.0 \times 10^{-5}\ cm^2\,s^{-1}$ at a fluence of 3×10^{15} He cm^{-2},

$D_0 = 4.0 \times 10^{-6}\ cm^2\,s^{-1}$ at a fluence of 3×10^{16} He cm^{-2}.

Table 6
Activation energy of helium thermal diffusion in UO_2

Method	3.0×10^{16} He cm^2	3.0×10^{15} He cm^2
Excitation curve [5]	1.9	2.1
SIMNRA ($E_d = 1270$ keV)	2.2	2
SIMNRA ($E_d = 1300$ keV)	2	2.2

These values are 2.5 and 5.5 orders of magnitude lower than the results measured in zirconolite [12] or britholite [5], respectively.

This value is fully comparable to the values previously obtained by release measurements or by thermal desorption experiments.

The linear regression used to determine the activation energy is characterized by a coefficient of determination R^2 between 0.95 and 0.989 for both curves. The activation energy is thus estimated within ±0.1 eV.

The activation energy for PuO_2 has been estimated as 2.38 eV [1], based on release measurements between 600 and 1900 °C. Extrapolating the preceding data shows that the diffusion value at 1200 °C is slightly higher than determined for UO_2 [3], i.e. $5.2\times10^{-17}\ m^2\,s^{-1}$ compared with $1.5\times10^{-17}\ m^2\,s^{-1}$ obtained by pressurized helium gas infusion.

This similarity is shown in Fig. 10, after mass correction on the diffusion coefficients, because radiogenic helium is ^{4}He, according to Eq. (6) often cited in the literature ([5,20]):

$$D(^4\text{He}) = D(^3\text{He}) \times \sqrt{\frac{3}{4}}. \tag{6}$$

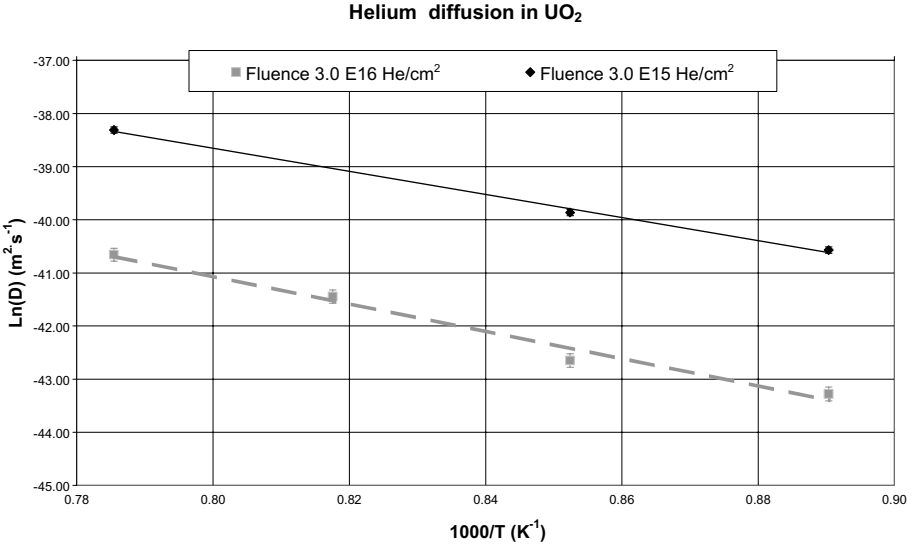

Fig. 9. Diffusion coefficient variation versus temperature in UO_2.

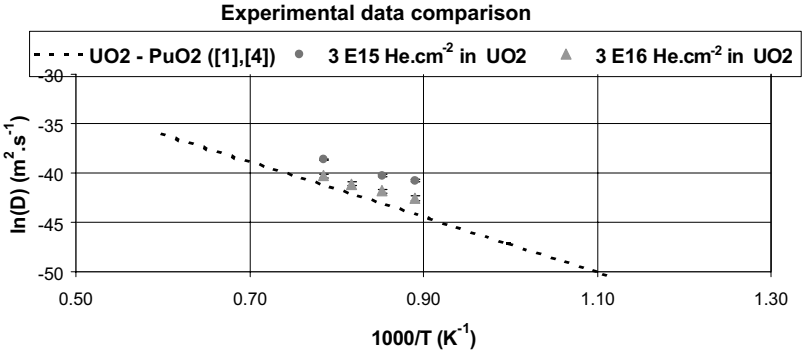

Fig. 10. Comparison of results obtained with published reports.

The thermal diffusion coefficients are very low compared with other matrices and particularly with nuclear glasses [6] for which the difference is nearly 10 orders of magnitude; these measurements also confirm the greater mobility of helium compared with fission gases and volatile fission products in the spent fuel matrix: the difference is two orders of magnitude compared with xenon diffusion [24]. Moreover, the activation energy is significantly lower for thermal diffusion of helium.

It may be of interest to note here that this value, about 2 eV, is close to the activation energy value of the migration of vacancies in UO_2. Further experiments are needed to understand the full mechanism implemented there.

3.3. Effect of implantation defects

When the helium ions were implanted a zone of vacancy defects was created preceding the peak, as simulated by SRIM2000. We attribute the shift in the implantation peaks toward the surface to the presence of these defects. This damage zone also enhanced diffusion via the defects: the diffusion coefficient was linked to the concentration of vacancy defects in the material. At the higher fluence, the concentration of implantation defects increases while a significant drop is observed in the measured diffusion coefficients; this can be attributed either to bubble formation or to a trapping/detrapping mechanism by interactions between He^+ ions and atomic defects, because of the uncertainty of the solubility limit value for helium in uranium dioxide.

Nevertheless, studies of the effects of ion implantation in UO_2 [25] show that at high doses the implantation of rare gas (Xe or Kr) results in gas trapping related to a strong interaction with the defects. Complete recovery is obtained only at high temperatures (above 1500 K). Conversely, for low doses thermal recovery is possible at temperatures below 870 K.

The activation energy found (about 2 eV) corresponds to vacancy-assisted diffusion. The measured diffusion coefficient D may be considered as an apparent diffusion coefficient including both diffusion and trapping processes. If Θ is the fraction of vacancies that are occupied and N_t the molar fraction of vacancies, and considering that trapping and detrapping follow first-order kinetics with rate constants k and k' respectively, we can write [26]:

$$D = \frac{D_L}{1 + KN_t(1-\Theta)^2}, \tag{7}$$

where $K = \frac{k}{k'}$.

Assuming that within the experimental temperature range, the same mechanisms occur in terms of trapping and detrapping, Eq. (7) may explain the decrease in D with the fluence, i.e. with increasing N_t. This assumes Θ is very small, i.e. that the system is far from saturation.

So, TEM observations of samples implanted at high doses with or without annealing will provide conclusive evidence of the origin of the differences in helium diffusion observed in the two types of implanted samples.

It should be noted, however, that helium implantation creates relatively minor damage in the matrix compared with Xe bombardment or with the damage that would be arise with the same helium concentration by disintegration (recoil nucleus and He^{2+} particle) in

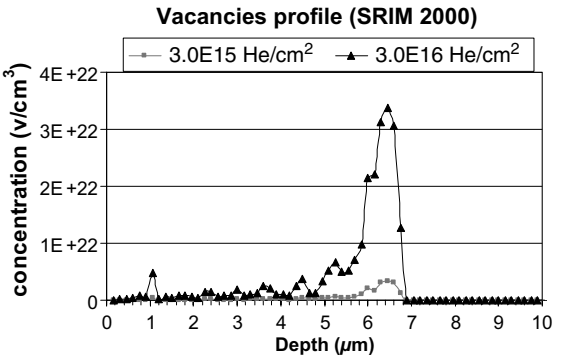

Fig. 11. Estimated vacancy defects created by ion implantation (SRIM 2000).

spent fuel. Furthermore, the results shown in Fig. 11, in terms of amount of atomic defects created, more than 10^{22} cm^{-3}, are overestimated by the SRIM 2000 code, not taking into account the vacancy-interstitials recombination.

At high fluence and for temperature of 1100 °C we thus deduced by extrapolation a diffusion coefficient of about 2.0×10^{-17} m^2 s^{-1}. This value is slightly lower but still in good correlation with the value determined by [27] using a more accurate numerical solution of Fick's equation based on NRA spectral data for samples implanted at a depth of about 2 μm.

4. Conclusion

This study has determined the thermal component of the helium-3 diffusion coefficient in uranium dioxide. It provides experimental confirmation that thermal diffusion is negligible within the time/temperature range of interim storage and disposal. After 2 billion years, this thermal migration under repository conditions should not exceed 10 μm (mean grain size).

Extrapolating data determined by other techniques at high temperature correlates well with the results obtained. So, at room temperature, the value of the diffusion coefficient is close to 10^{-41} m^2 s^{-1}.

The subsequent work in this study will consist in determining this coefficient under α self-irradiation, particularly the acceleration of diffusion by atomic defects generated by α disintegrations. Actinide-doped specimens are now being characterized for this purpose. Helium produced by α disintegration could be analyzed by a ^{4}He(p,p)^{4}He reaction if this method provides suitable performance, or local ^{3}He implantation in damaged materials.

Release experiments such as those described in [28] show that helium is released above 800 °C from actinide-doped UO_2 pellets. Formation of nanometer size bubbles is observed. Several experiments have shown similar behavior in spent fuel. Considering the diffusion coefficients determined here, the thermal component cannot account for this mobility. Additional experiments are planned with UO_2 pellets doped with ^{244}Cm, ^{238}Pu and ^{241}Am. Migration will be analyzed according to the quantity of helium generated and the damage level reached in the matrix.

Supplementary transmission electron microscopy observations will be carried out to determine whether or not helium precipitates in the form of bubbles, depending on the concentration and temperature.

Together, these studies will provide an overall assessment of helium behavior in the spent fuel matrix. Based on the repository characteristics (package dimensions and temperature), this parameter will allow us to estimate the quantities of helium released by packages under interim storage and disposal conditions, and to estimate the variation in the occluded helium fraction likely to induce physical and mechanical modifications in the matrix.

Acknowledgements

The authors are grateful to M. Plantier and M. Gardon from the IPN (Villeurbane) for their sample implantation work. Financial support for this research was provided under the CEA-PRECCI program (C. Poinssot and C. Ferry), and the CEA-CLTC Project (J.M. Cavedon), as part of CEA-EDF agreement (J.M. Gras).

References

[1] F. Rufeh, D.R. Olander, T.H. Pigford, Nucl. Sci. Eng. 233 (1965) 335.
[2] P. Sung, Equilibrium solubility and diffusivity of helium in single-crystal uranium oxide, PhD thesis, Univ. Washington, 1967.
[3] H.J. Matzke, Radiat. Eff. 64 (1982) 3.
[4] W.A. Stark, Sandia Laboratories Report, Albuquerque, New Mexico, p. 554.
[5] D. Gosset, P. Trocellier, Y. Serruys, J. Nucl. Mater. (2002).
[6] A.R. Hall, G.J. Wldrick, Measurement of helium diffusion coefficient in a simulated highly active waste storage glass, AERE-R8706, Mai 1977.
[7] P. Trocellier, D. Gosset, D. Simeone, J.M. Costantini, X. Deschanels, D. Roudil, Y. Serruys, R. Grynszpan, S. Saudé, M. Beauvy, in: Application of nuclear reaction for ^{3}He depth profiling in nuclear ceramics presented at IBMM 2002 conference in Kobe, Japan.
[8] P. Trocellier, D. Gosset, D. Simeone, J.M. Costantini, X. Deschanels, D. Roudil, Y. Serruys, R. Grynszpan, S. Saudé, M. Beauvy, Nucl. Instrum. and Meth. B 206 (2003) 1077.
[9] F. Paszti, Nucl. Instrum. and Meth. B 66 (1992) 83.
[10] P.P. Pronko, J.G. Pronko, Phys. Rev. B 9 (7) (1974) 2870.
[11] M. Hufschmidt, V. Heintze, W. Möller, D. Kamke, Nucl. Instrum. and Meth. B 124 (1975) 573.
[12] X. Deschanels, D. Roudil, S. Peuget, T. Advocat, D. Gosset, P. Trocellier, 'Détermination du coefficient de diffusion de l'hélium dans la zirconolite' Poster presented at 'MATERIAUX 2002' Conference, Tours (France), 21–25 October 2002.
[13] H.J. Matzke, J. Ottaviani, D. Pellotiero, J. Rouault, J. Nucl. Mater. 160 (1988) 142.
[14] B.V. Dobrov, V.V. Likhanskii, V.D. Orzin, A.A. Solodov, At. Energ. 82 (2) (1997).
[15] A. Nakamura, T. Fujino, J. Nucl. Mater. 140 (1986) 113.
[16] J.F. Ziegler, J.P. Biresack, U. Littmamark, The Stopping and Range of Ions in Solids, Pergammon, New York, 1985.
[17] M. Mayer, SIMNRA user's guide, Technical Report IPP 9/113, Max-Planck-Institute für Plasmaphysik, Garching, 1997.
[18] H.S. Bosh, G.M. Hale, Nucl. Fusion 32 (1992) 611.

[19] C. Gaillard, N. Chevarier, C. DenAuwer, N. Millard-Pinardn, P. Deichère, Ph. Sainsot, J. Nucl. Mater. 299 (2001) 43.
[20] J.M. Constantini, J.J. Grob, J. Haussy, P. Trocellier, Ph. Trouslard, J. Nucl. Mater. 321 (2003) 281.
[21] D.R. Olander, P. Van Uffelen, J. Nucl. Mater. 288 (2001) 137.
[22] A.H. Booth, Atomic Energy of Canada Ltd., Report AECL-496, 1957.
[23] S. Guilbert, T. Sauvage, H. Erranli, P. Desgradin, G. Blondiaux, C. Corbel, J.P. Piron, J. Nucl. Mater. 321 (2003) 121.
[24] H.J. Matzke, in: I.J. Hastings (Ed.), Advances in Ceramics 17, The American Ceramic Society Inc., Columbus, Ohio, 1986.
[25] H.J. Matzke, Turos, J. Nucl. Mater. 188 (1992) 285.
[26] J. Philibert, Ed Phys. (1985).
[27] S. Guilbert, T. Sauvage, Ph. Garcia, G. Carlot, M.-F. Barthe, P. Desgardin, G. Blondiaux, C. Corbel, J.P. Piron, He migration in implanted UO_2 sintered disks, J. Nucl. Mater., submitted for publication.
[28] V.V. Rondinella, T. Wiss, H.J. Matzke, J.P. Hiernaut, R. Fromknecht, in: Mass charge transport in ceramics materials: Fundamental to devices, 2000, p. 499.